



## Positive effects of $K^+$ in hybrid CoMn-K and Pd/Ba/Al<sub>2</sub>O<sub>3</sub> catalysts for NO<sub>x</sub> storage and reduction

Zhifeng Bai<sup>a</sup>, Bingbing Chen<sup>a</sup>, Qi Zhao<sup>a</sup>, Chuan Shi<sup>a,\*</sup>, Mark Crocker<sup>b,c,\*\*\*</sup>

<sup>a</sup> State Key Laboratory of Fine Chemicals, School of Chemistry, Dalian University of Technology, Dalian 116024, China

<sup>b</sup> Center for Applied Energy Research, University of Kentucky, Lexington, KY 40511, USA

<sup>c</sup> Department of Chemistry, University of Kentucky, Lexington, KY 40506, USA



### ARTICLE INFO

#### Keywords:

Potassium ions  
Hybrid catalyst  
NO<sub>x</sub> storage and reduction  
Non-thermal plasma

### ABSTRACT

CoMn-K was mechanically mixed with a Pd/Ba/Al<sub>2</sub>O<sub>3</sub> catalyst to enhance its NO<sub>x</sub> storage and reduction properties. The Pd/Ba/Al<sub>2</sub>O<sub>3</sub> and CoMn-K mixture showed a synergistic effect with respect to NO<sub>x</sub> storage capacity and improved NO<sub>x</sub> reduction ability. The addition of K<sup>+</sup> ions promoted the catalytic performance by increasing NO oxidation activity and therefore NO<sub>x</sub> storage via the creation of active surface oxygen species on the catalysts. The stored NO<sub>x</sub> reduction by H<sub>2</sub> was also improved, being ascribed to the fact that Pd was mainly present as Pd<sup>0</sup> due to the electronic interactions between Pd and K<sup>+</sup> ions. NO<sub>x</sub> conversions and N<sub>2</sub> selectivity at low temperatures (80–200 °C) could be further enhanced by assistance of non-thermal plasma in rich phase.

### 1. Introduction

NO<sub>x</sub> storage and reduction (NSR) is an effective method for removing NO<sub>x</sub> from automobile exhaust [1,2]. Traditional NSR catalysts (also known as lean NO<sub>x</sub> trap (LNT) catalysts) of the type Pt/Ba/Al<sub>2</sub>O<sub>3</sub> (PBA) exhibit low NO<sub>x</sub> removal efficiency below 300 °C. However, the temperature of automobile exhaust gas has been decreased with the improvement of fuel utilization efficiency. The exhaust temperature of light duty diesel vehicles is about 180–350 °C [3]. Moreover, during the cold start period, the exhaust temperature might even be lower than 200 °C [4,5]. Therefore, it is very important to improve the low temperature performance of LNT catalysts.

Numerous studies have focused on catalyst components which can potentially improve the activity of NO<sub>x</sub> storage and reduction at low temperature. Le Phuc et al. [6] showed that Mn doped in Pt/Ba/Al<sub>2</sub>O<sub>3</sub> induced different behaviors depending on the temperature. At low temperature (< 300 °C), Mn was poisonous for the reduction step, which was due to the interaction of Pt and Mn that inhibited the reduction of NO<sub>x</sub>. Kim et al. [7] found that Pt/Ba/Al<sub>2</sub>O<sub>3</sub> loaded with 2 wt % Co demonstrated high NO<sub>x</sub> uptake during lean cycles, however, the presence of Co caused the reduction efficiency during rich cycles to decrease, being ascribed to increased NO<sub>x</sub> release without reduction. In our previous studies, doping transition metal oxides (Co, Mn) into Pt (Pd)/Ba/Al<sub>2</sub>O<sub>3</sub> catalysts [3,8,9] or mechanically mixing perovskites with Pt/Ba/Al<sub>2</sub>O<sub>3</sub> catalyst [10] was similarly found to be an effective

approach to enhance NO<sub>x</sub> storage capacity at low temperatures. Nevertheless, the poor activity of such catalysts with respect to rich phase regeneration presents a problem for NSR catalysis, especially at low temperatures. However, high NO<sub>x</sub> conversions could be obtained when the catalysts with high NO<sub>x</sub> storage capacity associated with non-thermal plasma in rich phase to improve NO<sub>x</sub> reduction [11]. From these studies it emerged that maximizing NO<sub>x</sub> storage capacity is a key factor in plasma-assisted NSR if optimal NO<sub>x</sub> removal efficiency is to be realized.

NO oxidation is a crucial step in the NO<sub>x</sub> storage process because NO<sub>2</sub> is easier to store on the catalyst than NO [12]. Lots of inexpensive transition metal oxides are known to possess high activity in oxidation reactions (including NO oxidation) [13–15], manganese and cobalt oxides being among the most active. Likewise, as reported in our previous study [16], CoMn-oxide (Co<sub>2.25</sub>Mn<sub>0.75</sub>O<sub>4</sub>) catalyst is very active for HCHO and CO oxidation due to the presence of highly reactive surface oxygen. In addition, literature reports indicate that alkali metal ions can promote catalyst performance in such reactions. For example, Huang et al. [13] reported that the addition of K<sup>+</sup> ions to 3D - NiCo<sub>2</sub>O<sub>4</sub> nanosheets can promote catalytic activity in HCHO oxidation, which was attributed to the synergistic effect of the Co<sup>3+</sup>/Co<sup>2+</sup> and Ni<sup>3+</sup>/Ni<sup>2+</sup> redox cycles, as well as the presence of OH species on the catalyst surface. Fan et al. [17] showed that the Co<sup>3+</sup>/Co<sup>2+</sup> molar ratio was increased by employing KHCO<sub>3</sub> as the precipitant, thus further promoting HCHO oxidation. A study by Xu et al. [18] inferred that the

\* Corresponding author at: State Key Laboratory of Fine Chemicals, School of Chemistry, Dalian University of Technology, Dalian 116024, China.

\*\* Corresponding author at: Center for Applied Energy Research, University of Kentucky, Lexington, KY 40511, USA.

E-mail addresses: [chuansi@dlut.edu.cn](mailto:chuansi@dlut.edu.cn) (C. Shi), [mark.crocker@uky.edu](mailto:mark.crocker@uky.edu) (M. Crocker).

isolated potassium atoms on a K/hollandite manganese oxide (HMO) catalyst possessed hybridized d-sp orbitals and high electron density, thereby promoting oxygen activation and enhancing low-temperature catalytic activity in the complete oxidation of HCHO and ethyl acetate.

Based on the above results, we selected CoMn-oxide modified with K<sup>+</sup> ions as the oxidation component, mixed with Pd/Ba/Al<sub>2</sub>O<sub>3</sub>, to obtain high NSR activity. Owing to its relatively low cost and better tolerance to CO, there is a broad prospect to use Pd in commercial applications. Although Pd is comparatively active for NO<sub>x</sub> reduction, its NO oxidation ability is poor [19]. Accordingly, we used mechanical mixing method to prepare hybrid bi-functional catalysts to boost NSR activity and the effect of catalyst doping with K<sup>+</sup> was studied in the present work.

## 2. Experimental

### 2.1. Catalyst preparation

1%Pd/20%Ba/Al<sub>2</sub>O<sub>3</sub> (PBA) was prepared by the incipient wetness method as described in detail elsewhere [2]. The Mn<sub>0.75</sub>Co<sub>2.25</sub>O<sub>4</sub> (CoMn) catalyst was synthesized by a co-precipitation method [16]. The resulting CoMn (0.2 g) was immersed in an aqueous solution of KOH (1 M, 100 mL) at 80 °C. After stirring for 5 h, the catalyst was filtered and washed with water, and then dried at 60 °C. The resulting catalyst is denoted as CoMn-K. The CoMn/CoMn-K + PBA catalysts were prepared by mixing equal masses of each component by means of grinding, followed by calcination at 500 °C for 4 h in air.

### 2.2. Catalyst characterization

Elemental compositions were determined by digesting the samples in mixed acids, followed by analysis using inductively coupled plasma-atomic emission spectroscopy (ICP-AES).

Catalyst basicity was measured by CO<sub>2</sub>-TPD. The catalysts (50 mg) was pre-treated at 200 °C for 1 h in Ar, and then the catalyst was exposed to 1% CO<sub>2</sub>/Ar (100 ml/min) at 100 °C for 60 min, followed by Ar purging for another 30 min, after which the temperature was increased to 700 °C at a heating rate of 10 °C/min in flowing of Ar (200 ml/min). The CO<sub>2</sub> concentration was monitored by non-dispersive infrared absorption spectrometer (SICK-MAIHAKS710, Germany).

XRD analysis of samples was carried on an X-ray diffractometer (Rigaku D-Max Rotaflex) using a Cu K $\alpha$  radiation source in a 2θ range of 10–80°.

H<sub>2</sub>-TPR measurements were used an AutoChem II 2920 chemisorption analyzer (Micromeritics, USA). 50 mg of sample was first purged with Ar at 200 °C for 1 h, followed by cooling to room temperature. The sample was then heated from room temperature to 800 °C at a rate of 10 °C min<sup>-1</sup> under flowing 5% H<sub>2</sub>/Ar (50 ml·min<sup>-1</sup>).

BET surface area analysis was performed with a JW-BK 122 W system using N<sub>2</sub> as the probe molecule.

Scanning transmission electron microscopy (STEM) images of as-prepared catalysts were taken on a Tecnai F30 microscope in the dark field.

X-ray photoelectron spectroscopic (XPS, ESCALAB250, Thermo GV, USA) analysis was conducted using Al K $\alpha$  X-rays as the excitation source operating at 15 kV and 10 mA. Binding energies were referenced to the C 1 s signal at 284.6 eV.

CO chemisorption was conducted on a diffuse reflectance infrared Fourier transform (DRIFT) spectrometer (Bruker-Tensor-27, Germany) equipped with a mercury cadmium tellurium (MCT) detector. The pretreated sample was pulsed with a gas mixture of 3% CO/He at room temperature.

### 2.3. In situ DRIFTS of NO<sub>x</sub> storage and reduction

In situ diffuse reflectance infrared Fourier transform spectroscopy

(DRIFTS) measurements were performed on a Tensor 27 (Bruker) FTIR spectrometer. The catalyst was first pretreated in 5% H<sub>2</sub>/Ar at 500 °C for 30 min and then cooled to the desired temperature in He. During the storage process, the gas mixture (either 500 ppm NO/8% O<sub>2</sub>/He, 500 ppm NO/50 ppm SO<sub>2</sub>/8% O<sub>2</sub>/He, or 50 ppm SO<sub>2</sub>/8% O<sub>2</sub>/He) was fed to the DRIFTS cell for 25 min, after which the cell was purged with He for another 15 min at the same temperature. All spectra were obtained with a resolution of 4 cm<sup>-1</sup> and 60 scans.

For temperature programmed surface reaction (TPSR) studies, the catalyst sample was first exposed to 500 ppm NO/8% O<sub>2</sub>/He at 300 °C for 1 h, then purged with He and cooled to 100 °C. After that, the sample was heated from 100 °C to 300 °C under flowing 3% H<sub>2</sub>/Ar. Spectra were recorded in 50 °C increments up to 300 °C by averaging 60 scans.

### 2.4. Catalytic properties

NO<sub>x</sub> storage capacity (NSC) and NO oxidation capacity (NOC) experiments were performed in a microreactor under lean conditions as a function of temperature using a chemiluminescence NO<sub>x</sub> analyzer (Ecotech ML9841AS) as the detector. Prior to each measurement, the catalyst (150 mg) was pretreated in 5% H<sub>2</sub>/Ar at 500 °C for 1 h. Steady-state NO oxidation was measured using 500 ppm NO/8% O<sub>2</sub>/2% CO<sub>2</sub>/2% H<sub>2</sub>O/Ar as the feed in the range 150–400 °C. The NO conversion was calculated as follows:

$$\text{NOC} = \frac{C_{\text{NO}_2,\text{out}}}{C_{\text{NO},\text{in}}} \times 100\% \quad (1)$$

NSC measurements were performed by exposing the pretreated catalyst to the same atmosphere as the NO oxidation experiment. The storage time was 50 min. To investigate the influence of CoMn-K addition on sulfur tolerance, the samples were sulfated by exposure to 500 ppm NO/8% O<sub>2</sub>/50 ppm SO<sub>2</sub>/2% H<sub>2</sub>O/2% CO<sub>2</sub>/Ar balance at 300 °C for 50 min. The NSC was calculated according to the following formula:

$$\text{NSC} = \frac{\int_0^t (C_{\text{NO}_x,\text{in}} - C_{\text{NO}_x,\text{out}}) dt}{m} \quad (2)$$

where t is the NO<sub>x</sub> storage time, m is the mass of the catalyst, C<sub>NO<sub>x</sub>,in</sub> and C<sub>NO<sub>x</sub>,out</sub> is the NO<sub>x</sub> concentration in the feed gas and in the outlet gas, respectively.

NO<sub>x</sub>-TPD measurements were conducted with 150 mg of catalyst to study the stability of adsorbed NO<sub>x</sub> species. The catalyst was first pre-reduced with 5% H<sub>2</sub>/Ar at 500 °C for 60 min and cooled down to 200 °C in flowing Ar. The sample was then exposed to 500 ppm NO, 8% O<sub>2</sub>, 2% H<sub>2</sub>O, 2% CO<sub>2</sub>/Ar at 200 °C for 50 min, followed by Ar purging for another 30 min, after which the temperature was increased to 700 °C at a heating rate of 10 °C/min in flowing Ar. The exhaust gas was monitored on line by a mass spectrometer (Pfeiffer Vacuum GSD 301).

Temperature programmed surface reduction (H<sub>2</sub>-TPSR) was conducted as follows: the sample was first treated in 5% H<sub>2</sub>/Ar at 500 °C for 1 h, after which NO<sub>x</sub> adsorption was performed for 50 min at 300 °C. The sample was then allowed to cool to room temperature under flowing Ar. Next, the feed gas was switched to 2% H<sub>2</sub>/Ar and the sample was heated to 500 °C at a rate of 10 °C/min. The exhaust gas was monitored on line by a mass spectrometer (Pfeiffer Vacuum GSD 301).

NSR performance was evaluated using either a quartz reactor or a dielectric-barrier discharge (DBD) reactor loaded with 150 mg catalyst. The activity was investigated under alternating rich and lean atmospheres. The reactor effluent was analyzed online by a mass spectrometer (Pfeiffer Vacuum GSD 301) and a FTIR (Sick Maihak S710). Before the activity assessment, the catalyst was pretreated in 5% H<sub>2</sub>/Ar at 500 °C for 1 h. Further details of the experiments are summarized in Table S1. Once stationary cycling conditions had been attained, NO<sub>x</sub> conversion and N<sub>2</sub> selectivity were calculated as follows, using the

average values obtained from 5 cycles:

$$\text{NO}_x \text{ conversion} = \frac{\int_0^t (C_{\text{NO}_{x,\text{in}}} - C_{\text{NO}_{x,\text{out}}})dt}{\int_0^t C_{\text{NO}_{x,\text{in}}} dt} \times 100\% \quad (3)$$

$$\text{N}_2 \text{ selectivity} = \frac{\text{NO}_{x,\text{in}} - \text{NO}_{x,\text{out}} - \text{NH}_{3,\text{out}} - 2\text{N}_2\text{O}_{\text{out}}}{\text{NO}_{x,\text{in}} - \text{NO}_{x,\text{out}}} \quad (4)$$

In the NTP-assisted experiments, energy consumption was calculated as follows:

$$\text{Energy consumption (mmol NO}_x/\text{W}\cdot\text{h}) = \frac{n_{\text{NO}_{x,\text{in}}} \times x_{\text{NO}_x \text{ conversion}}}{P \times t} \quad (5)$$

where  $P$  is the discharge power and  $t$  is discharge time.

The  $\text{NO}_x$  storage efficiency (NSE) in lean phase and the percentage of  $\text{NO}_x$  released (NRE) in rich phase during lean-rich cycling were calculated as follows:

$$\text{NSE} = \frac{\int_0^t (C_{\text{NO}_{x,\text{in}}} - C_{\text{NO}_{x,\text{out}}})dt}{\int_0^t C_{\text{NO}_{x,\text{in}}} dt} \times 100\% \quad (6)$$

$$\text{NRE} = \frac{\text{NO}_x \text{ released in rich purge}}{\text{NO}_x \text{ stored in lean phase}} \times 100\% \\ = 1 - \frac{\text{NO}_x \text{ conversion}}{\text{NSE}} \quad (7)$$

The poisoning effect of  $\text{SO}_2$  on the catalysts was also investigated. The catalysts were sulfated by exposing to a feed gas containing 100 ppm  $\text{SO}_2$ /8%  $\text{O}_2/\text{Ar}$  for 60 min at 300 °C, and then measuring catalyst performance under lean - rich cycling without  $\text{SO}_2$  in the feed as described above.

### 3. Results

#### 3.1. Catalyst characterization

As shown in Table 1, the ICP-AES data show that for the hybrid catalysts (CoMn + PBA, CoMn-K + PBA), the Pd content is almost half of that in the PBA catalyst, as expected. The surface area for PBA is 102  $\text{m}^2/\text{g}$ , while the surface areas of CoMn + PBA and CoMn-K + PBA are similar. In addition, the amount of  $\text{CO}_2$  desorption (calculated from  $\text{CO}_2$ -TPD shown in Fig. S1) on CoMn-K + PBA is much larger (1.07 mmol/g) than that on CoMn + PBA catalyst (0.34 mmol/g), suggesting that the introduction of  $\text{K}^+$  enhances the basicity of the sample.

To investigate the effect of alkali addition on the structure of CoMn, the XRD patterns of CoMn and CoMn-K were investigated. As shown in

**Table 1**

Summary of ICP-AES, BET,  $\text{CO}_2$ -TPD, Pd particle size and XPS data for as-prepared catalysts.

	PBA	CoMn + PBA	CoMn-K + PBA
Pd (wt%)	0.93	0.57	0.59
K (wt%)	N/A	N/A	1.5
BET ( $\text{m}^2/\text{g}$ )	102	98	96
$\text{CO}_2$ -TPD <sup>a</sup> (mmol/g)	0.33	0.34	1.07
Pd particle size <sup>b</sup> (nm)	3.14	N/A	3.07
$\text{Co}^{3+}/\text{Co}^{2+}$	N/A	0.862	1.381
$\text{Mn}^{4+}/\text{Mn}^{3+}$	N/A	0.902	0.555
$\text{Pd}^{2+}/\text{Pd}^0$	0.507	2.468	0.247
$\text{O}_{\text{ads}}/\text{O}_{\text{latt}}$	0.559	1.69	2.03

<sup>a</sup> Desorption amount of  $\text{CO}_2 = \frac{\int_0^t C_{\text{CO}_2,\text{out}} dt}{m}$ , where  $t$  is the  $\text{CO}_2$  desorption time,  $m$  is the mass of the catalyst,  $C_{\text{CO}_2,\text{out}}$  is the  $\text{CO}_2$  concentration in the outlet gas, respectively.

<sup>b</sup> Average value of 200 Pd particles in STEM image.

Fig. 1(A), a diffraction pattern characteristic of  $\text{Co}_3\text{O}_4$  can be clearly observed for the CoMn catalyst; however, there is no diffraction peak ascribable to manganese compounds. As indicated in the slow scan XRD pattern from 35.5° to 38.5° (Fig. S2), the shift of the (311) diffraction peak to lower 2θ angle is observed for CoMn with respect to  $\text{Co}_3\text{O}_4$  [20]. The lattice constant calculated for  $\text{Co}_3\text{O}_4$  is 8.068 Å, while that for CoMn is 8.096 Å. The lattice expansion (2θ decreasing) occurred due to the replacement of  $\text{Co}^{3+}$  (0.61 Å) in the spinel structure by  $\text{Mn}^{3+}$  (0.65 Å) with a slightly larger radius [21]. The above results confirm the formation of a Co-Mn-O solid solution. When CoMn is modified with KOH, apart from the major  $\text{Co}_3\text{O}_4$  phase, the presence of  $\text{K}_6(\text{Mn}_2\text{O}_6)$  is detected (inset of Fig. 1(A)), implying a chemical interaction of K and Mn.

XRD analysis also provided structural information for the PBA, CoMn + PBA and CoMn-K + PBA samples (Fig. 1(B)). In the case of PBA, two distinct peaks are observed, identified as  $\text{BaCO}_3$  (JCPDS No. 45-1471) and  $\gamma\text{-Al}_2\text{O}_3$  (JCPDS No. 47-1770). XRD analysis shows that the major diffraction peaks present in the PBA + CoMn and PBA + CoMn-K catalysts are  $\text{BaCO}_3$ ,  $\gamma\text{-Al}_2\text{O}_3$  and  $\text{Co}_3\text{O}_4$  (JCPDS No. 74-2120). Notably, after mechanical mixing, a new phase  $\text{Ba}_3\text{CoO}_5$  appears and the peak intensity of  $\text{BaCO}_3$  weakens, indicating a strong chemical interaction of CoMn and Ba/ $\text{Al}_2\text{O}_3$  during calcination.

In order to investigate the effects of  $\text{K}^+$  doping on the redox properties of CoMn + PBA,  $\text{H}_2$ -TPR experiments were performed, the resulting profiles being shown in Fig. 2. The  $\text{H}_2$  consumption peak of PBA is not clearly observed due to the low concentration of  $\text{PdO}_x$ . Two major  $\text{H}_2$  consumption peaks are observed for hybrid catalysts, the first peak being assigned to the reduction of  $\text{Co}^{3+}$  to  $\text{Co}^{2+}$  overlapped with the reduction of  $\text{Mn}^{4+}$  to  $\text{Mn}^{3+}$ , while the latter belongs to the reduction of  $\text{Co}^{2+}$  to  $\text{Co}^0$  and  $\text{Mn}^{3+}$  to  $\text{Mn}^{2+}$  [3,16]. Compared with CoMn + PBA catalyst, the first consumption peak shifts to higher temperature due to the formation of the  $\text{K}_6(\text{Mn}_2\text{O}_6)$  phase which leads to a change in the chemical valence of Mn. This has been further confirmed by XPS results shown in Fig. S3.

To study possible variations in the morphology of the Pd particles in PBA, CoMn + PBA and CoMn-K + PBA, STEM analysis was performed. As displayed in Fig. 3(A), the PBA sample is characterized by small Pd particles of 3.14 nm. After mechanical mixing (Fig. 3(B)), the Pd nanoparticles are difficult to detect, may be due to the presence of  $\text{Pd}^{6+}$ . Interestingly, when the CoMn sample is modified with KOH, the individual bright spots which correspond to Pd nanoparticles are clearly seen, as shown in Fig. 3(C).

XPS was used to analyze the surface chemical states of as-prepared catalysts, the results are shown in Fig. S3 and Table 1. The O 1s spectra of the PBA, CoMn + PBA and CoMn-K + PBA samples are shown in Fig. S3(A). By performing peak-fitting deconvolution, the results of different oxygen species distribution have been given in Table 1. Two oxygen species are present, with one peak located at BE (binding energy) = 530.0–530.7 eV, corresponding to lattice oxygen ( $\text{O}_{\text{latt}}$ ) species, and the other peak at BE = 531.4–532.0 eV ascribed to adsorbed oxygen species ( $\text{O}_{\text{ads}}$ ) [8,22,23]. As shown in Table 1, the ratio of  $\text{O}_{\text{ads}}/\text{O}_{\text{latt}}$  is 1.69 and 2.03 for PBA + CoMn and PBA + CoMn-K, respectively, these values being higher than for PBA (0.559) and implying that the amount of surface oxygen species are increased after mechanical mixing. Moreover, the ratio of  $\text{O}_{\text{ads}}/\text{O}_{\text{latt}}$  is higher for the CoMn-K + PBA sample than that for CoMn + PBA, which can be attributed to the effect of alkali doping. This result suggests that doping with  $\text{K}^+$  creates active  $\text{O}_{\text{ads}}$ , which may be beneficial for NO oxidation.

XPS spectra in the Co 2p and Mn 2p regions show spin-orbit splitting of the 2p signal into 2p1/2 and 2p3/2 components, as shown in Fig. S3(B) and (C). Curve-fitting reveals that the Co 2p3/2 signal has two components at BE = 779.5 and 780.7 eV, which indicate the presence of  $\text{Co}^{3+}$  and  $\text{Co}^{2+}$  species [24], respectively. Mn 2p3/2 signals are observed at BE values of 641.5 and 643.2 eV, the former corresponding to  $\text{Mn}^{3+}$  [23,25], whereas the latter originates from  $\text{Mn}^{4+}$  [26]. Quantitative analysis pertaining to the ratio of  $\text{Co}^{3+}/\text{Co}^{2+}$  and  $\text{Mn}^{4+}/$

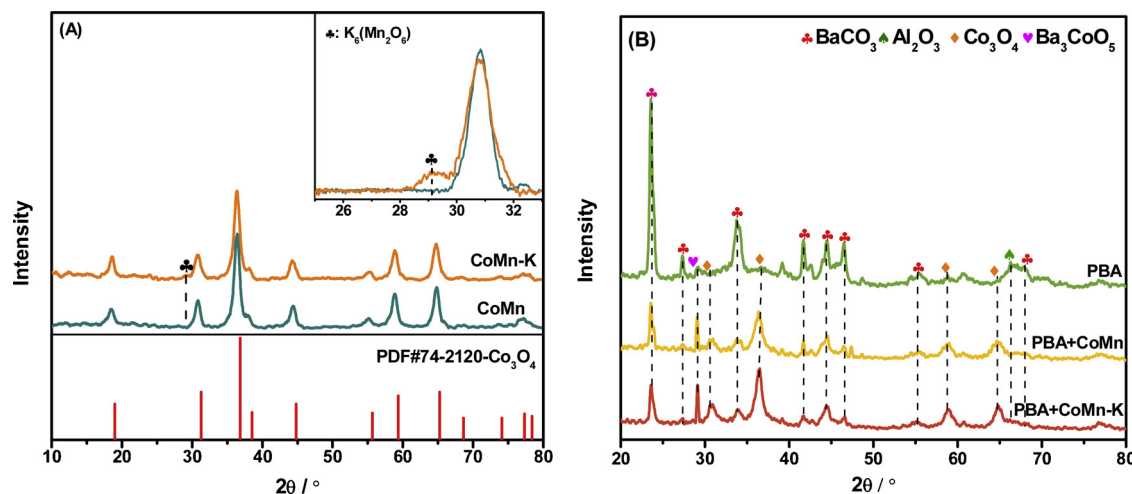


Fig. 1. XRD patterns of catalysts: (A) CoMn, CoMn-K; (B) PBA, CoMn + PBA, CoMn-K + PBA.

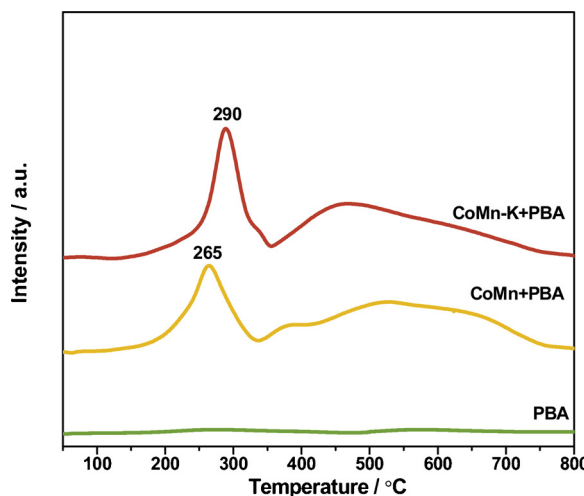


Fig. 2. H<sub>2</sub>-TPR profiles obtained at a rate of 10 °C/min under flowing 5% H<sub>2</sub>/Ar.

$\text{Mn}^{3+}$  is summarized in Table 1. The  $\text{Co}^{3+}/\text{Co}^{2+}$  ratio for CoMn-K + PBA (1.381) is larger than that of CoMn + PBA (0.862), while the  $\text{Mn}^{4+}/\text{Mn}^{3+}$  ratio of CoMn-K + PBA (0.555) is lower than that of CoMn + PBA (0.902). This finding can be explained by the occurrence of  $\text{K}^+$  at vacancy sites in  $\text{MnO}_x$  having a strong interaction with O, therefore the Mn-O bonds are weakened [14]. As a consequence, the charge ability of the  $\text{Mn}^{4+}$  decreased, and the amount of  $\text{Mn}^{3+}$  increased accordingly, this is consistent with the results of H<sub>2</sub>-TPR.

The K 2p XPS spectrum of CoMn-K + PBA is displayed in Fig. S3(D). The spectrum can be resolved into two peaks which can be ascribed to the K-O group, the main one at BE = 292.5 eV for K 2p3/2 being accompanied by satellite peaks at BE = 295.3 eV corresponding to the K 2p1/2 level [27]. According to the literature, theoretical calculations indicate that electron-rich potassium atoms are energetically favorable for dissociation of  $\text{O}_2$  by charge transfer from potassium to  $\text{O}_2$  [14,18]. As a result, more facile dissociative adsorption of  $\text{O}_2$  can account for higher content of  $\text{O}_{\text{ads}}$  species in the CoMn-K + PBA sample, as indicated by the XPS analysis.

Due to the low Pd content, the XPS signal to noise ratio for Pd is poor (as shown in Fig. S4). Therefore, DRIFTS measurements were performed after CO chemisorption on the PBA, CoMn + PBA and CoMn-K + PBA samples to investigate the state of the Pd (shown in Fig. 4). For each sample, bands could be observed in the region 2400–2300 cm<sup>-1</sup>, assigned to gaseous  $\text{CO}_2$ , and in the region 1800–

1100 cm<sup>-1</sup> assigned to carbonate species [28–30]. For PBA, a band at 1974 cm<sup>-1</sup> can be assigned to bridged CO species adsorbed on  $\text{Pd}^0$  sites [28,31], and another band at 2084 cm<sup>-1</sup> is assigned to CO linearly adsorbed on  $\text{Pd}^0$  [28]. After mechanical mixing, in addition to the aforementioned bands, a new band appeared at 2127 cm<sup>-1</sup> for the CoMn + PBA catalyst [28], which is ascribed to CO chemisorbed on  $\text{Pd}^{2+}$ , which in turn is indicative of charge transferred from Pd to CoMn mixed oxide. However, for the CoMn-K + PBA sample the CO band at 2127 cm<sup>-1</sup> is not detected, suggesting that addition of  $\text{K}^+$  inhibits the oxidation of Pd, i.e., Pd remains in the metallic state.

### 3.2. $\text{NO}_x$ storage and reduction

#### 3.2.1. NO oxidation and $\text{NO}_x$ storage capacity

In the  $\text{NO}_x$  storage process,  $\text{NO}_2$  is more easily stored on the catalyst than NO, so NO oxidation is one of key steps in the NSR reaction [32]. The conversion of NO to  $\text{NO}_2$  over PBA, CoMn + PBA and CoMn-K + PBA catalysts is shown in Fig. 5(A). Compared with PBA, NO oxidation activity is markedly higher for the CoMn + PBA and CoMn-K + PBA catalysts, suggesting that the CoMn/CoMn-K component in the hybrid samples contributes remarkably to the NO oxidation capacity, especially for CoMn-K. Combined the results of the XPS and NOC data, which can be inferred that surface oxygen plays a key role in catalytic NO oxidation.

The results of  $\text{NO}_x$  storage capacity measurements performed on the catalysts are shown in Fig. 5(B). It can be seen that the NSC of PBA increases along with temperature, which can be attributed to the high thermal stability of  $\text{Ba}(\text{NO}_3)_2$  [2,33]. Notably,  $\text{NO}_x$  storage capacity is significantly improved over the whole temperature range for the CoMn + PBA and CoMn-K + PBA samples compared with PBA, indicating that increasing NO oxidation activity via the addition of the CoMn and CoMn-K mixed oxides has a positive effect on  $\text{NO}_x$  storage. Moreover, a volcano-like dependence of  $\text{NO}_x$  uptake is observed for the CoMn-containing catalysts, with a maximum uptake of 604  $\mu\text{mol/g}$  for  $\text{NO}_x$  storage at 300 °C. This may be attributed to the lower thermal stability of nitrate on the catalysts which caused by the addition of the CoMn and CoMn-K oxides.

The  $\text{SO}_2$  resistance of hybrid catalyst was also studied.  $\text{NO}_x$  storage was performed over PBA and CoMn-K + PBA using the same feed as used for the foregoing experiments but with 50 ppm  $\text{SO}_2$  added. As shown in Table 2, in both cases the measured NSC declined. In the absence of  $\text{SO}_2$  the NSCs of PBA and CoMn-K + PBA at 300 °C are 273 and 604.8  $\mu\text{mol/g}$ , respectively, which decreased to 120.5 and 561.6  $\mu\text{mol/g}$  in the presence of  $\text{SO}_2$ . As detailed elsewhere, the poisoning effect of  $\text{SO}_2$  is a consequence of sulfate formation [34,35]. It

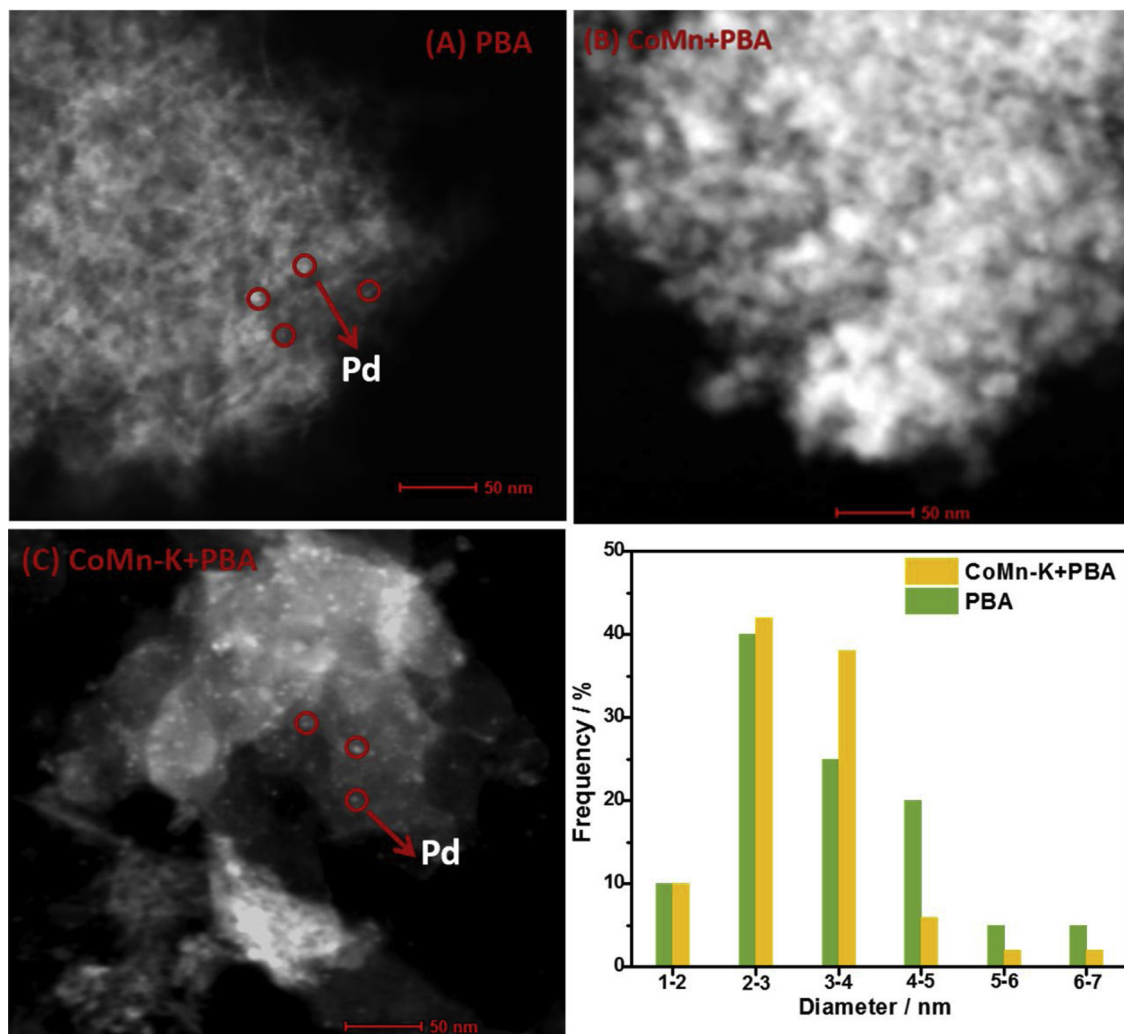


Fig. 3. STEM images of PBA, CoMn + PBA and CoMn-K + PBA catalysts and corresponding Pd particle size distributions.

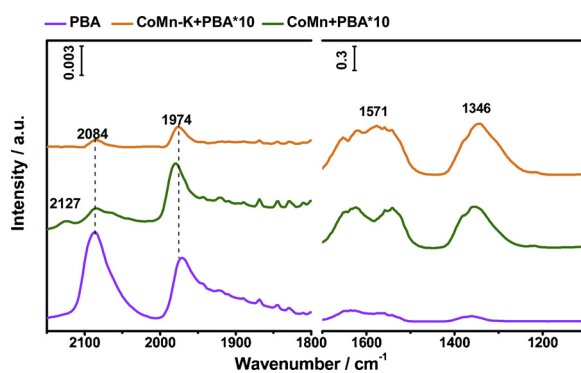


Fig. 4. In situ DRIFT spectra of CO adsorbed on catalysts at 20 °C.

should be noted that the NSC of CoMn-K + PBA in the presence of  $\text{SO}_2$  is higher than that of PBA under the same conditions, thus indicating that the addition of CoMn-K helps to mitigate the effect of sulfur poisoning.

### 3.2.2. $\text{NO}_x$ -TPD

$\text{NO}_x$ -TPD was performed from 200 to 700 °C to provide information concerning the nature of the adsorbed  $\text{NO}_x$  species on the catalysts. Fig. S5(A) shows the resulting  $\text{NO}_x$  concentration profiles for the PBA, CoMn + PBA and CoMn-K + PBA catalysts. Compared with PBA, the

amount of the  $\text{NO}_x$  desorption on CoMn + PBA and CoMn-K + PBA are obviously increased, which is in line with the result that NSC is enhanced on the hybrid catalysts.

Table 3 shows the  $\text{NO}_x$  storage efficiency of the catalysts in different temperature regions determined from deconvolution of the  $\text{NO}_x$ -TPD curves (Fig. S5(B)–(D)). In all cases two desorption peaks (375 and 490 °C) are observed for the catalysts. The first peak can be ascribed to  $\text{NO}_x$  release from  $\text{NO}_x$  stored on the  $\text{Al}_2\text{O}_3$  and/or Ba nitrate/nitrite species close to metal sites, while the latter peak can be assigned to the decomposition of Ba nitrates located far from Pd sites [8]. It is noticeable that for PBA a comparatively greater fraction of the stored  $\text{NO}_x$  is desorbed in the high temperature region than for CoMn + PBA and CoMn-K + PBA, indicating that when CoMn / CoMn-K is physically mixed with PBA, the thermal stability of the nitrates on the BaO is decreased. However, when the CoMn is modified with KOH and mixed with PBA, the thermal stability of the nitrates is better than for CoMn + PBA, indicating that the addition of  $\text{K}^+$  is beneficial for nitrate stability. We also utilize the DRIFTS to further improve the aforementioned results (as shown in Fig. S6).

### 3.2.3. Characterization of adsorbed $\text{NO}_x$ species by *in situ* DRIFTS

To understand the  $\text{NO}_x$  storage process, DRIFTS measurements were performed on PBA, CoMn + PBA and CoMn-K + PBA catalysts. As shown in Fig. 6, after PBA is exposed to  $\text{NO}/\text{O}_2/\text{Ar}$  at 200 °C for 25 min, three peaks are observed, which can be ascribed to nitrite species on Ba sites ( $1230 \text{ cm}^{-1}$ ) [12], monodentate nitrates associated with Al or Ba

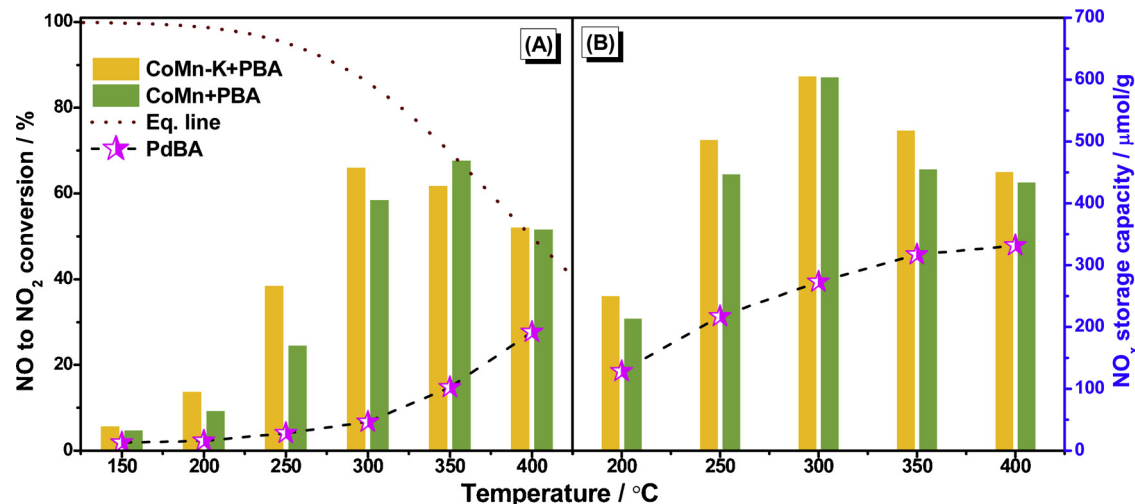


Fig. 5. (A) NO conversion to NO<sub>2</sub> measured under lean conditions (500 ppm NO, 8% O<sub>2</sub>, 2% CO<sub>2</sub> and 2% H<sub>2</sub>O, N<sub>2</sub> balance, GHSV = 100,000 h<sup>-1</sup>). (B) NO<sub>x</sub> storage capacities (NSCs) measured under lean conditions (500 ppm NO, 8% O<sub>2</sub>, 2% CO<sub>2</sub> and 2% H<sub>2</sub>O, Ar balance, 50 min storage, GHSV = 48,000 ml g<sup>-1</sup> h<sup>-1</sup>).

sites (1541 cm<sup>-1</sup>) and nitrates on Ba sites (1310 cm<sup>-1</sup>). The latter two peaks gradually increased in intensity with increasing temperature, implying the transformation of nitrites to nitrates. Upon exposure of the CoMn + PBA sample to the NO/O<sub>2</sub>/Ar mixture at 200 °C, bidentate nitrates on Ba (1310 cm<sup>-1</sup>), ionic nitrates on Ba sites (1350 cm<sup>-1</sup>) [36,37] and monodentate nitrates on Al (1556 cm<sup>-1</sup>) [1] are detected. Notably, the nitrite band (1230 cm<sup>-1</sup>) associated with the PBA component of the CoMn + PBA sample is no longer observed, which is likely a consequence of the stronger oxidation activity of CoMn + PBA compared to PBA. At 300 °C, the Ba ionic nitrate band at 1350 cm<sup>-1</sup> becomes the dominant species after storing NO<sub>x</sub> for 25 min. CoMn-K + PBA exhibits similar DRIFT spectra to CoMn + PBA, although the Ba nitrate signals are much stronger than for CoMn + PBA. This result can be due to the higher NO oxidation performance of CoMn-K + PBA arising from the addition of K<sup>+</sup>.

The effect of SO<sub>2</sub> on PBA and CoMn-K + PBA was also investigated by in situ DRIFTS. When the feed gas contained SO<sub>2</sub>, the results (Fig. 7(B)) are different from the results obtained in the absence of SO<sub>2</sub> (Fig. 7(A)). After PBA is exposed to SO<sub>2</sub>/O<sub>2</sub>/NO/Ar for 25 min, peaks attributed to sulfate species appear in the range 900–1100 cm<sup>-1</sup> [35], and the nitrite peak at 1230 cm<sup>-1</sup> and nitrate peak at 1301 cm<sup>-1</sup> gradually decrease in intensity. Notably, the DRIFT spectrum of CoMn-K + PBA is different to that of PBA, peaks attributed to sulfate species associated Ba species (900–1100 cm<sup>-1</sup>) are not observed. Meanwhile the intensity of bands at 1308, 1350 and 1540 cm<sup>-1</sup> increases with time - on stream, being attributed to adsorbed nitrate species [1,36]. The stronger intensity peak with respect to nitrate species over CoMn-K + PBA than over PBA catalyst is in accordance with its improved NSC (Fig. 5). From these, it seems that SO<sub>2</sub> shows less poison on NO<sub>x</sub> capture ability when CoMn-K is mixed with PBA catalyst.

In order to verify whether or not SO<sub>2</sub> is readily adsorbed on CoMn-K instead of on PBA, the PBA, CoMn-K and CoMn-K + PBA catalysts were exposed to SO<sub>2</sub>/O<sub>2</sub>/Ar at 300 °C, separately. As shown in Fig. S7, for PBA, peaks appear in the 1000–1400 cm<sup>-1</sup> range that can be assigned to sulfite and sulfate species associated with Ba species [32]. The DRIFT

Table 3

NO<sub>x</sub> desorption efficiency of catalysts at different temperatures.

Catalysts	200–400 °C (%)	400–700 °C (%)
CoMn + PBA	61.9	38.1
CoMn-K + PBA	49.6	50.4
PBA	38.7	61.3

spectrum of CoMn-K + PBA is similar with that of CoMn-K, but quite different with that of PBA. Peaks attributed to sulfate species associated Ba species (900–1100 cm<sup>-1</sup>) are not observed. The strong bands at 1260 cm<sup>-1</sup> and 1154 cm<sup>-1</sup> appeared, which should be attributed to sulfate species preferentially associated with CoMn-K oxide [38,39]. These results indicate that the addition of CoMn-K helps to mitigate the effect of sulfur poisoning and protect Pd/Ba/Al catalyst.

### 3.2.4. Reduction of adsorbed NO<sub>x</sub> species by H<sub>2</sub>

For purpose of clarifying the effect of K<sup>+</sup> on NO<sub>x</sub> reduction, the reduction of NO<sub>x</sub> stored on CoMn + PBA and CoMn-K + PBA was studied by H<sub>2</sub>-TPSR experiments. The results are shown in Fig. 8(A) and (B), signals corresponding to *m/z* = 2 (H<sub>2</sub>), *m/z* = 14 (N<sub>2</sub>), *m/z* = 15 (NH<sub>3</sub>) and *m/z* = 30 (released NO or fragmentation of N<sub>2</sub>O) being tracked. For CoMn + PBA (Fig. 8a), an obvious H<sub>2</sub> consumption peak is observed at 243 °C with simultaneous formation of NH<sub>3</sub> and N<sub>2</sub>O. The spectra in Fig. 10b is collected under H<sub>2</sub> atmosphere at increasing temperature after NO<sub>x</sub> adsorption. The IR absorption bands present in the spectra are those corresponding to Ba nitrate (1353, 1384 and 1540 cm<sup>-1</sup>), the intensity of the bands is observed to decrease along with temperature raise. Mass spectrometric data and DRIFT spectra acquired for CoMn-K + PBA during H<sub>2</sub>-TPSR are shown in Fig. 8(B). The spectra for CoMn-K + PBA catalyst is examined over 100–300 °C, it is obviously observed that the reduction temperature of nitrate species adsorbed on CoMn-K + PBA is lower than that on CoMn + PBA, for the more obvious decrease in intensity of nitrate bands at 1355 cm<sup>-1</sup> compared with the initial intensity at 100 °C (as shown in Fig. 8d). This

Table 2

NO<sub>x</sub> storage capacities (NSCs) measured under lean conditions and NO<sub>x</sub> conversion in the presence/absence of SO<sub>2</sub> at 300 °C.

Catalysts	NSC (μmol/g)		NO <sub>x</sub> conversion (%)		NSE (%)	
	Fresh	Sulfated	Without SO <sub>2</sub>	With SO <sub>2</sub>	Without SO <sub>2</sub>	With SO <sub>2</sub>
PBA	273.0	120.5	47.6	18.0	62.4	20.2
CoMn-K + PBA	604.8	561.6	91.7	71.2	99.0	76.5

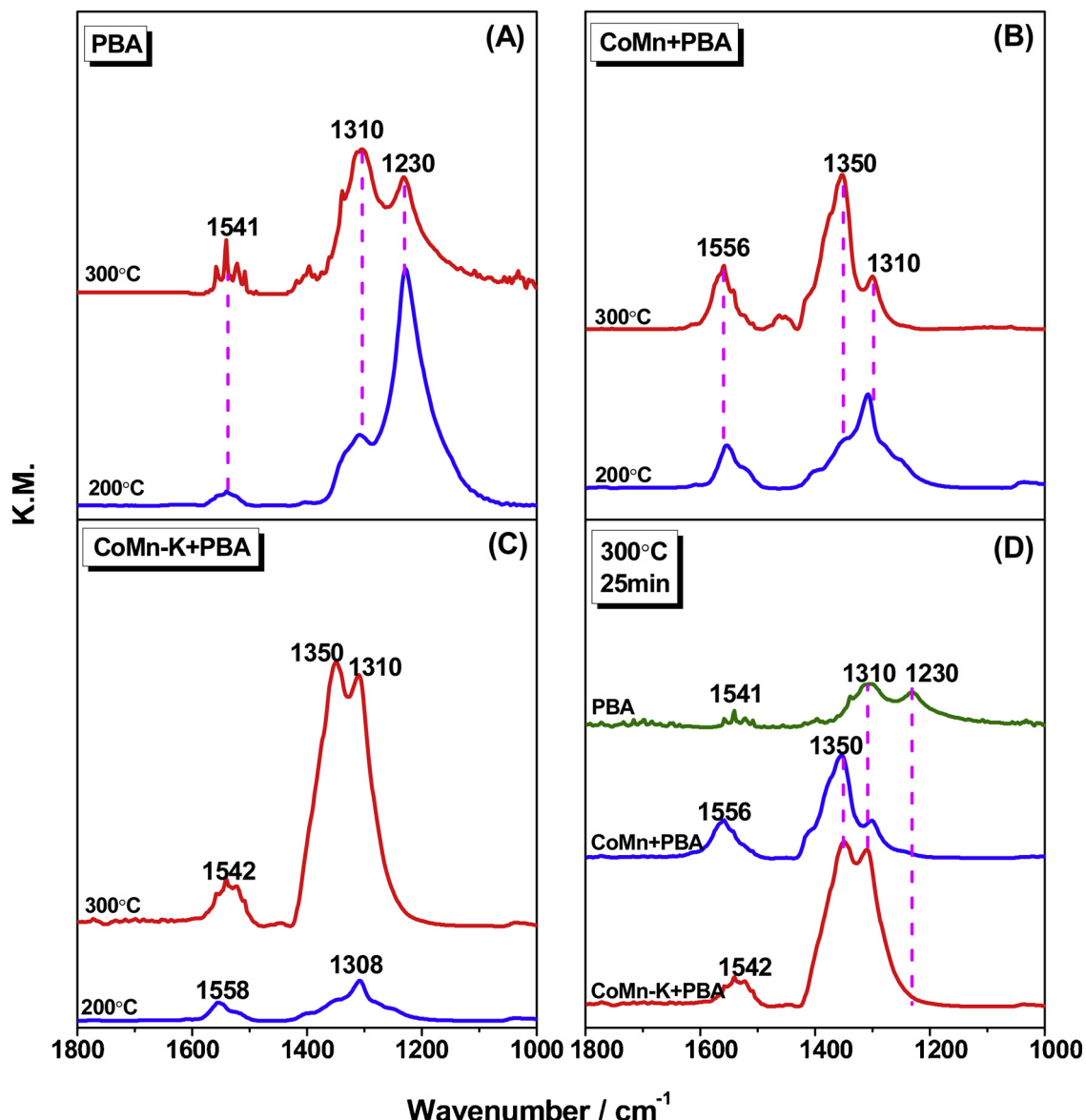


Fig. 6. In situ DRIFT spectra of (A) PBA, (B) CoMn + PBA and (C) CoMn-K + PBA after 25 min NO adsorption at different temperatures and (D) all catalysts after 25 min NO adsorption at 300 °C.

finding is consistent with the results of TPSR, in which  $\text{NO}_x$  stored on CoMn-K + PBA is found to be more reactive to reduction with  $\text{H}_2$  as compared to CoMn + PBA (an obvious  $\text{H}_2$  consumption peak being observed at 204 °C for CoMn-K + PBA), suggesting that the addition of  $\text{K}^+$  improves  $\text{NO}_x$  reduction activity.

### 3.2.5. Cycled $\text{NO}_x$ storage and reduction

The  $\text{NO}_x$  conversions and the  $\text{NO}_x$  concentration profiles over as-prepared catalysts are shown in Fig. 9 and S8. For PBA catalyst, the  $\text{NO}_x$  conversion increases along with temperature. In the case of hybrid catalysts, the activity increases at first and then decreases with the increase of temperature, the maximum  $\text{NO}_x$  conversion of 92% is obtained over CoMn-K + PBA during 250–300 °C. Notably, the CoMn-K + PBA sample possesses higher  $\text{NO}_x$  conversion compared with CoMn + PBA, which can be ascribed to the positive effects of  $\text{K}^+$  on  $\text{NO}_x$  storage and reduction (as shown in Fig. 5 and Fig. 8).

The cycle-averaged lean phase  $\text{NO}_x$  storage efficiency (NSE) and rich phase  $\text{NO}_x$  release efficiency (NRE) values are collected in Table 4. Comparing the NSE for the three samples, it can be clearly found that the NSE values of CoMn + PBA and CoMn-K + PBA are higher than

that of PBA above 150 °C, the  $\text{K}^+$  promoted CoMn catalyst having the highest NSE values. All the hybrid samples show increased NSE at first and then decreased with increasing temperature, in contrast, the highest NSE value on PBA is obtained at 400 °C as 62.2%. This again emphasizes that BaO is favorable for  $\text{NO}_x$  storage at higher temperature, while addition of the CoMn mixed oxide decreases the thermal stability of nitrates. As to the NRE values, the CoMn + PBA catalyst is higher than that for CoMn-K + PBA, which suggests that the addition of  $\text{K}^+$  is beneficial for the  $\text{NO}_x$  reduction activity of catalyst. Combined NRE and NSE data, the addition of  $\text{K}^+$  not only improves the  $\text{NO}_x$  storage capacity, but also promotes the reduction of  $\text{NO}_x$  and facilitates the regeneration of the catalyst.

The reaction rate at 150 °C over PBA, CoMn + PBA and CoMn-K + PBA catalysts which measured under kinetic regions (external diffusion being excluded) are  $172.8 \mu\text{mol}_{\text{NO}} \cdot \text{mol}_{\text{Pd}}^{-1} \text{h}^{-1}$ ,  $194.4 \mu\text{mol}_{\text{NO}} \cdot \text{mol}_{\text{Pd}}^{-1} \text{h}^{-1}$  and  $291.6 \mu\text{mol}_{\text{NO}} \cdot \text{mol}_{\text{Pd}}^{-1} \text{h}^{-1}$ , respectively. This result clearly demonstrates that the introduction of  $\text{K}^+$  indeed has a positive effect on the catalytic performances of CoMn-K + PBA catalyst in the NSR reaction.

As mentioned above, CoMn + PBA and CoMn-K + PBA catalysts



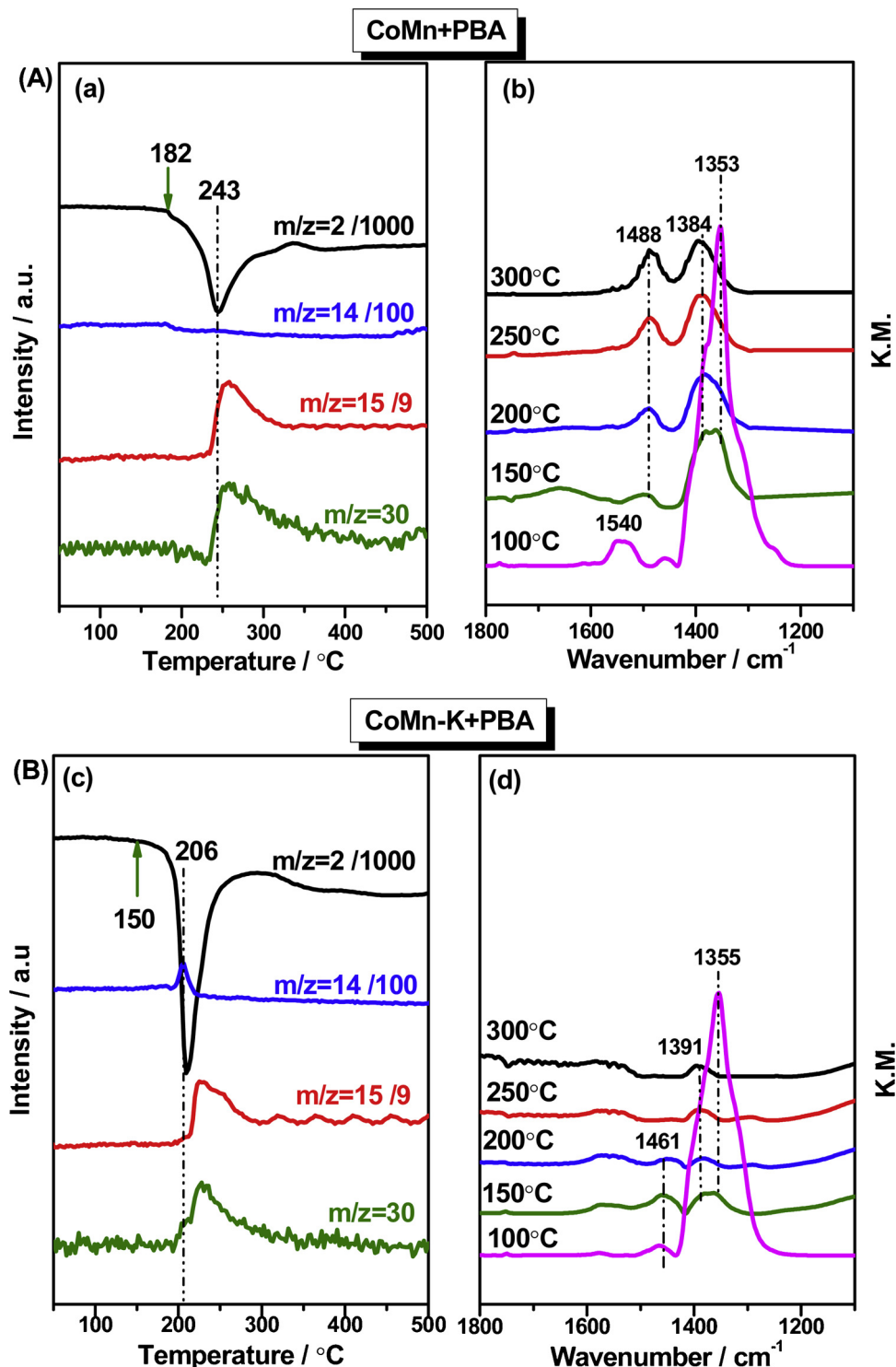


**Fig. 8.** MS (a, c) and DRIFT spectral data (b, d) for CoMn + PBA (A) and CoMn-K + PBA (B) catalysts in 3% H<sub>2</sub>/Ar after NO adsorption using 500 ppm NO/8% O<sub>2</sub>/2% H<sub>2</sub>O/2% CO<sub>2</sub>/Ar for 50 min; NO adsorption was performed at 300 °C.

show relatively low activity in NO<sub>x</sub> storage-reduction cycling process at low temperatures (< 250 °C), which may be ascribed to NO<sub>x</sub> reduction limitation in rich phase. Based on the previous studies [9–11], we intended to utilize the non-thermal plasma in the rich phase to improve the low temperature activity, as indicated in Fig. 10. The corresponding NO<sub>x</sub> concentration profiles are shown in Fig. S9. From the results in Fig. 10, the NO<sub>x</sub> conversion of all the samples is evidently improved over the temperature range tested. For PBA, the NO<sub>x</sub> removal efficiency is still lower than hybrid catalysts, which is owing to the comparatively

lower NO<sub>x</sub> storage capacity. In the case of CoMn-K + PBA, the NO<sub>x</sub> conversion is more than 70% within the temperature range 80–200 °C. It is also noticeable that even under H<sub>2</sub>-plasma conditions, the NO<sub>x</sub> conversion is poorer over CoMn + PBA than over CoMn-K + PBA. The results of CO chemisorption and STEM reveal that the Pd exists in an oxidized state on the CoMn + PBA sample. Therefore, even in an H<sub>2</sub>-plasma assisted NO<sub>x</sub> reduction process, NO<sub>x</sub> reduction efficiency of CoMn + PBA is lower than CoMn-K + PBA catalyst.

As shown in Table 5, under the H<sub>2</sub>-plasma assisted process, the

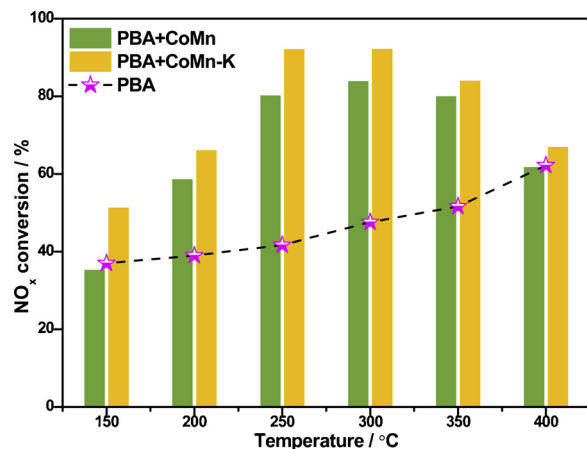


Fig. 9. NO<sub>x</sub> conversion during lean/rich cycling at different temperatures (lean phase: 500 ppm NO/8% O<sub>2</sub>/2% H<sub>2</sub>O/2% CO<sub>2</sub>/Ar, duration: 5 min; rich phase: 2% H<sub>2</sub>/2% H<sub>2</sub>O/2% CO<sub>2</sub>/Ar, duration: 1 min, GHSV = 80,000 h<sup>-1</sup>).

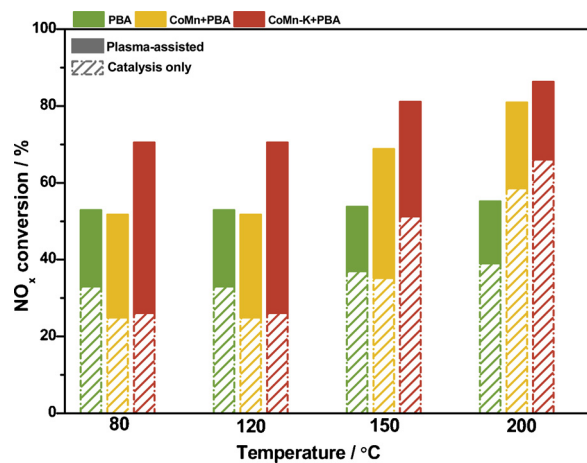


Fig. 10. NO<sub>x</sub> conversion during lean/rich cycling at 80 and 200 °C (lean phase: 500 ppm NO/8% O<sub>2</sub>/2% H<sub>2</sub>O/2% CO<sub>2</sub>/Ar, duration: 5 min; rich phase: 2% H<sub>2</sub>/2% H<sub>2</sub>O/2% CO<sub>2</sub>/Ar, duration: 1 min, P = 1.8 W, GHSV = 80,000 h<sup>-1</sup>).

Table 4

Comparison of NO<sub>x</sub> storage, release and selectivity of N<sub>2</sub>, NH<sub>3</sub> and N<sub>2</sub>O during NO<sub>x</sub> storage/reduction cycling.

Temp. (°C)	Catalysts	NO <sub>x</sub> conv. (%)	NSE (%)	NRE (%)	N <sub>2</sub> select. (%)	NH <sub>3</sub> select. (%)	N <sub>2</sub> O select. (%)
80	PBA	17.08	38.36	55.45	74.61	7.35	18.05
	PBA + CoMn	10.26	33.90	69.75	65.70	4.96	29.35
	PBA + CoMn-K	11.33	35.09	67.71	72.91	0.00	27.09
120	PBA	33.00	53.12	37.13	67.42	11.24	21.32
	PBA + CoMn	24.92	43.55	42.78	69.12	18.59	12.29
	PBA + CoMn-K	26.07	45.56	42.78	80.81	7.05	12.40
150	PBA	37.00	53.42	29.01	58.31	36.33	5.31
	PBA + CoMn	35.24	53.32	33.77	62.46	29.71	7.84
	PBA + CoMn-K	51.20	63.75	19.68	50.03	49.94	0.00
200	PBA	39.00	57.43	32.09	68.74	28.81	2.43
	PBA + CoMn	58.58	67.99	13.23	49.89	50.11	0.00
	PBA + CoMn-K	65.86	72.23	8.82	38.70	61.30	0.00
250	PBA	41.71	58.21	28.34	77.05	19.67	3.28
	PBA + CoMn	80.17	84.33	4.07	77.90	16.74	5.36
	PBA + CoMn-K	91.62	98.32	6.81	89.21	10.68	0.00
300	PBA	47.61	62.43	23.74	77.38	19.55	3.07
	PBA + CoMn	83.84	94.25	10.22	90.92	2.68	6.39
	PBA + CoMn-K	91.67	98.98	7.38	98.23	1.60	0.00
350	PBA	51.61	65.01	20.61	82.6	16.23	1.16
	PBA + CoMn	84.73	93.7	8.73	96.31	0.76	2.93
	PBA + CoMn-K	80.00	96.95	17.48	98.66	1.20	0.00
400	PBA	62.22	72.83	14.57	91.26	8.31	0.43
	PBA + CoMn	61.74	87.61	29.00	96.11	1.00	2.90
	PBA + CoMn-K	67.00	91.47	26.75	99.07	0.84	0.00

CoMn-K + PBA has higher NSE and lower NRE than CoMn + PBA and PBA catalysts, and its NSE value has been greatly improved which is increased from 11.3% to 69.9% at 80 °C in the presence of NTP. This indicates that the addition of plasma can promote the reduction of NO<sub>x</sub> to regenerate the catalyst, thereby improving subsequent lean phase performance.

The impact of SO<sub>2</sub> on catalytic activity was also studied and the results are shown in Table 2. For the poisoned PBA and CoMn-K + PBA, the NO<sub>x</sub> conversion is 18.0% and 71.2% at 300 °C, respectively, which is lower than the conversions obtained on the fresh catalysts (47.6% for PBA and 91.7% for CoMn-K + PBA). This is ascribed to decreased NO<sub>x</sub> storage efficiency as a consequence of catalyst sulfation. However, the NSE and NO<sub>x</sub> conversion values are significantly higher over CoMn-K + PBA than over PBA catalyst, indicating that the addition of CoMn-K apparently improves the sulfur tolerance.

The volatile nature of K, due to the low melting point (334 °C) of KNO<sub>3</sub>, as well as its high solubility in water, gives rise to technical challenges in avoiding the loss of K from LNT catalysts [40,41]. XRD data show that a new phase, K<sub>6</sub>(Mn<sub>2</sub>O<sub>6</sub>), is formed upon addition of KOH to CoMn, which provides a potential means of stabilizing K. In order to verify whether K is lost or not after reaction, the stability of the CoMn-K + PBA catalyst was evaluated. From data collected at 300 °C, as shown in Table S2, it can be observed that upon repeated use of the catalyst in NO<sub>x</sub> storage and reduction from 150 to 400 °C (i.e., three runs in which cycling was performed starting at 150 °C and ending at 400 °C), the NO<sub>x</sub> conversion and NO<sub>x</sub> storage efficiency are almost unchanged. At the same time, the content of K in the fresh and the spent CoMn-K + PBA catalyst measured by ICP-AES remained unchanged at 1.5%. Evidently, the strong interaction between K and CoMn does indeed help to decrease the mobility of K.

### 3.2.6. Product selectivity

The product selectivity is summarized and shown in Table 4. For PBA, the N<sub>2</sub> selectivity is 58.3% at 150 °C, increasing to 82.6% at 350 °C, and 91.3% at 400 °C. In comparison, the selectivity of N<sub>2</sub> reaches 96.1% and 99.1% for CoMn + PBA and CoMn-K + PBA, respectively, at 400 °C. The increase in N<sub>2</sub> selectivity along with temperature comes at the expense of N<sub>2</sub>O and NH<sub>3</sub> selectivity, both of which exhibit the highest values in the 80–200 °C. In the case of N<sub>2</sub>O formation, mixing CoMn with PBA actually results in slightly increased

**Table 5**Comparison of  $\text{NO}_x$  storage, release and selectivity of  $\text{N}_2$ ,  $\text{NH}_3$  and  $\text{N}_2\text{O}$  during plasma-assisted  $\text{NO}_x$  storage/reduction cycling.

Temp. (°C)	Catalysts	$\text{NO}_x$ conv. (%)	NSE (%)	NRE (%)	$\text{N}_2$ select. (%)	$\text{NH}_3$ select. (%)	$\text{N}_2\text{O}$ select. (%)
80	PBA	49.16	65.65	25.10	87.00	0.00	13.00
	PBA + CoMn	51.12	64.35	20.56	92.75	0.00	6.78
	PBA + CoMn-K	69.86	75.85	7.90	94.13	0.00	5.88
120	PBA	51.23	67.32	21.34	92.04	0.00	8.04
	PBA + CoMn	51.71	65.09	20.55	94.75	0.00	5.26
	PBA + CoMn-K	70.53	76.76	8.12	94.88	0.00	5.12
150	PBA	53.00	67.32	37.31	100.00	0.00	0.00
	PBA + CoMn	68.83	79.62	13.54	94.30	0.00	5.70
	PBA + CoMn-K	81.12	83.69	3.06	100.00	0.00	0.00
200	PBA	54.00	65.65	34.50	98.60	1.40	0.00
	PBA + CoMn	80.89	89.23	9.34	93.22	0.00	6.78
	PBA + CoMn-K	86.34	88.68	2.63	100.00	0.00	0.00

$\text{N}_2\text{O}$  make at high temperatures (250–400 °C) compared to PBA. Interestingly, the  $\text{N}_2\text{O}$  yield is negligible when the CoMn is modified with KOH, indicating that the addition of  $\text{K}^+$  suppresses  $\text{N}_2\text{O}$  formation.

The effects of plasma on the product distribution are shown in Table 5. In general, the  $\text{N}_2$  selectivity increases for all the samples with the addition of  $\text{H}_2$ -plasma in the rich phase, the effect being larger at lower temperatures. Moreover, the  $\text{N}_2$  selectivity value is higher over CoMn-K + PBA than for CoMn + PBA, suggesting a synergistic effect of  $\text{K}^+$  and plasma leading to improved  $\text{N}_2$  selectivity. The effect of plasma on  $\text{N}_2$  selectivity is readily demonstrated by the results obtained for PBA: at 150 °C, the  $\text{N}_2$  selectivity (100%) is obviously higher than that acquired without NTP assistance during the rich phase (58.3%), the selectivity to  $\text{NH}_3$  and  $\text{N}_2\text{O}$  being 36.3% and 5.3%, respectively, in the latter case. Hence, introducing  $\text{H}_2$ -plasma in the rich phase provides an effective approach to improve  $\text{N}_2$  selectivity at low temperatures.

#### 4. Discussion

In this work, coupling non-thermal plasma with a NSR catalyst enabled the removal of  $\text{NO}_x$  at temperatures lower than 200 °C. However, for practical applications it is crucial to minimize the fuel consumption in plasma-assisted  $\text{NO}_x$  storage-reduction, which in turn necessitates enhancing the  $\text{NO}_x$  storage capacity of the NSR catalyst. In the present study, CoMn-K was mechanically mixed with Pd/Ba/ $\text{Al}_2\text{O}_3$  catalyst to enhance both  $\text{NO}_x$  storage and reduction properties. The origin of the resulting synergy is discussed below.

##### 4.1. Effects of mechanically mixed CoMn-K and Pd/Ba/ $\text{Al}_2\text{O}_3$ catalysts on $\text{NO}_x$ storage capacity

Previous studies have shown that Pd exhibits good  $\text{NO}_x$  reduction ability, but the NO oxidation ability is poor [8]. However, increasing the rate of NO oxidation by mechanically mixing CoMn-K oxide with Pd/Ba/ $\text{Al}_2\text{O}_3$  provides the opportunity to increase NSR catalyst activity and potentially decrease the amount of Pd required in the catalyst.

In the case of the CoMn-K + PBA catalyst, its high NO oxidation activity can mainly be attributed to the contribution of CoMn-K component. Due to the abundant surface oxygen of transition metal oxide [16], the ratio of  $\text{O}_{\text{ads}}/\text{O}_{\text{latt}}$  on CoMn-K + PBA is much higher than that for PBA which is known from XPS result. Specifically, the excellent oxidation properties of the mixed oxide [42] promoted  $\text{NO}_2$  formation and therefore improved the  $\text{NO}_x$  storage efficiency of the CoMn-K + PBA catalyst. The re-dispersion of  $\text{BaCO}_3$  phase has been demonstrated by the weak reflections in XRD which is due to interaction of  $\text{BaCO}_3$  with CoMn-K. In relation to the storage mechanism, the proximity of the sites responsible for NO oxidation (CoMn-K) to the  $\text{NO}_x$  trapping sites (Ba) should influence NO and  $\text{O}_2$  spill-over [8]. Indeed, the limiting step for Pt/Ba/ $\text{Al}_2\text{O}_3$  catalysts during lean-rich cycling is believed to be transfer of  $\text{NO}_x$  between Pt and Ba, hence the proximity between the Pt and Ba phases can significantly impact the  $\text{NO}_x$  spillover

from Pt to Ba during  $\text{NO}_x$  storage and in turn  $\text{NO}_x$  spillover from Ba to Pt during  $\text{NO}_x$  reduction [43]. This suggests that the promoting effect of CoMn-K not only derives from its high NO oxidation activity, but is also related to the intimate contact of CoMn-K with Ba. This should result in a large interfacial contact area between CoMn-K and Ba/ $\text{Al}_2\text{O}_3$ , thus directly accelerating nitrite/nitrate formation.

It is well known that  $\text{SO}_2$  and NO form competitive adsorption on the storage site Ba, generating  $\text{BaSO}_4$ , leading to the deactivation of the catalyst [44]. Therefore, in the present work, we have prepared hybrid catalyst CoMn-K + PBA to mitigate the effects of sulfur poisoning and protect the traditional catalyst PBA. As  $\text{SO}_2$  is present in the lean phase, the NSC of CoMn-K + PBA is higher than that of PBA under the same conditions (shown in Table 2). Such improvement in  $\text{NO}_x$  storage capacity can be further evidenced by DRIFTS, the sulfates species are easily occurred on the storage sites Ba and therefore reduce the  $\text{NO}_x$  storage sites. After combining the CoMn-K oxides with PBA, sulfate species preferentially associated with CoMn-K oxide as shown in Fig. S7, from these, it seems that  $\text{SO}_2$  shows less poison on  $\text{NO}_x$  capture ability when CoMn-K is mixed with PBA catalyst as shown in Fig. 7. From the above, it is obvious that mixing PBA with CoMn-K oxide enhanced the  $\text{NO}_x$  storage capacity of catalyst in the presence of  $\text{SO}_2$ .

##### 4.2. Effect of $\text{K}^+$ doping on NSR

In order to investigate how the addition of  $\text{K}^+$  affects the physico-chemical properties of the catalyst and thus affects the activity of NSR, we investigated the structure and surface properties of the catalyst by XRD,  $\text{H}_2$ -TPR, STEM, XPS and CO chemisorption to reveal the essence of the excellent properties of the hybrid catalyst.

Owing to the addition of  $\text{K}^+$  ions, XRD data show that a new phase  $\text{K}_6(\text{Mn}_2\text{O}_6)$  is formed, which will cause a change in the valence state of Co and Mn, thereby affecting the surface adsorption oxygen. This result has been further proved by  $\text{H}_2$ -TPR, the low temperature reduction peak of CoMn-K + PBA catalyst shifts to higher temperature, which belongs to the formation of  $\text{K}_6(\text{Mn}_2\text{O}_6)$  and increases the content of  $\text{Mn}^{3+}$ . XPS data show that the CoMn-K + PBA catalyst exhibits higher  $\text{Co}^{3+}/\text{Co}^{2+}$  ratio, lower  $\text{Mn}^{4+}/\text{Mn}^{3+}$  and more surface adsorbed oxygen species than CoMn + PBA. The above results show that the addition of  $\text{K}^+$  can produce more surface oxygen species, which process high activity in oxidation reactions. According to the results of  $\text{CO}_2$ -TPD, the introduction of  $\text{K}^+$  improves the surface basicity on the hybrid catalyst. Moreover, differences are observed in the Pd oxidation state in the mixed catalysts. In the case of CoMn, mechanical mixing with PBA changes the chemical valence of the Pd. Specifically, an electronic interaction arises between Pd and the CoMn component as evidenced by the presence of  $\text{Pd}^{2+}$ . However, after mixing with CoMn-K, the chemical state of Pd remain in metallic state as confirmed by the results of CO chemisorption and STEM, which is attributed to donation of electron from K. Therefore, the addition of  $\text{K}^+$  enables the active component of Pd being in a metallic state of  $\text{Pd}^0$ .

Correlating these structural properties with NSR performance, it is clear that:

- (1) For NSC: due to the abundant surface oxygen species, CoMn-K + PBA exhibits better NO oxidation activity and therefore enhanced NSC as compared with CoMn + PBA. Moreover, the NSC at high temperature is enhanced as a consequence of the enhanced thermal stability of nitrate associated with the strongly basic K<sup>+</sup> ions.
- (2) For NO<sub>x</sub> reduction: the reduction of stored NO<sub>x</sub> is also promoted. NO<sub>x</sub> adsorbed on CoMn-K + PBA is reduced at lower temperatures than on CoMn + PBA. This is related to the reduced state of the Pd, presumably arising from electron transfer from K. The metallic state of Pd is essential for H<sub>2</sub> adsorption and dissociation. As a consequence, CoMn-K + PBA exhibits superior NO<sub>x</sub> reduction properties during rich phase purging.
- (3) For product selectivity: in contrast to CoMn + PBA, N<sub>2</sub>O is not produced during the regeneration phase above 150 °C for the CoMn-K + PBA catalyst. This may be ascribed to the fact that metallic Pd<sup>0</sup> species facilitate NO dissociation, i.e., Pd-NO + Pd → Pd-N + Pd-O and 2Pd-N → N<sub>2</sub> + 2Pd [19]. Another way of looking at this is to consider N<sub>2</sub>O formation on Pt-containing NSR catalysts, multiple studies having shown that under lean-rich cycling N<sub>2</sub>O is mainly formed in the rich reaction front, in a process which must proceed in close association with removal of oxygen from the surface of the metal particles via reaction with the reductant [45,46]. Under these conditions, the local H<sub>2</sub>/NO stoichiometry at Pt is low, due to the simultaneous consumption of reductant by stored oxygen, including that on the oxidized Pt particles, and by the released NO<sub>x</sub>. At low temperature (< 200 °C) low reductant/NO<sub>x</sub> ratios are known to favor the formation of N<sub>2</sub>O [47]. Likewise, it can be expected that N<sub>2</sub>O selectivity over Pd-containing NSR catalysts will be dependent on the oxidation state of the Pd.

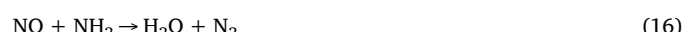
#### 4.3. Non-thermal plasma enhanced NSR performance

NO<sub>x</sub> storage and reduction (NSR) technology is constrained at low temperatures, such that in practice a significant amount of NO<sub>x</sub> is slipped through the aftertreatment system when catalyst temperatures are below ~200 °C. Such low temperatures are associated with cold-start emissions and can constitute a major portion of the total NO<sub>x</sub> emitted during a drive cycle. One strategy to overcome this low temperature limitation is to couple electrically-produced non-thermal plasmas (NTPs) with heterogeneous catalysts.

It is evident that CoMn-K + PBA shows better regeneration properties in plasma-assisted rich phase purging than in the absence of plasma, the NSE on CoMn-K + PBA during plasma-assisted lean-rich cycling being double that stored in the absence of plasma-assisted purging at 80 °C. This is consistent with our previous research [3,9], in which it was found that the NO<sub>x</sub> conversion was improved when H<sub>2</sub>-plasma introduced in rich phase. Significantly, the application of NTP in the rich phase provides the most energy efficient approach for coupling NSR catalysts with plasma, since the discharge time is relatively short compared to the storage phase. The energy consumption as 0.495–0.636 mmol/Wh which is comparable with literature results gained over CoMn-K + PBA [3,48]. In other words, the energy penalty of 35.06–45.09 Wh is required to remove the 500 ppm NO<sub>x</sub> in 1 m<sup>3</sup> combustion gas.

In addition, it is noteworthy that the N<sub>2</sub> selectivity is improved in H<sub>2</sub>-plasma as compared to the catalysis-only system. NH<sub>3</sub> and H<sub>2</sub> are activated easily by non-thermal plasma because of their low bond energies (H<sub>2</sub>: ca. 4.4 eV; NH<sub>3</sub>: ca. 3.9 eV) [3,49]. It has been reported that the concentration of radicals and excited species formed by electron collisions in Ar gas is around 2–4 orders of magnitude higher than that of the ions. Therefore, ammonia, hydrogen and argon free radical species can be generated and reduction reactions may take place in the

system as follows [48,50,51]:



where H<sub>2</sub><sup>\*</sup>, Ar<sup>\*</sup> are excited molecules of H<sub>2</sub> and Ar, O<sup>\*</sup> is excited O radicals.

On this basis, the superior selectivity of H<sub>2</sub>-containing plasma for NSR regeneration and NO<sub>x</sub> reduction can be ascribed to the enhanced formation of radical species in the plasma and the ability of H, NH<sub>2</sub>, NH and Ar<sup>\*</sup> to directly participate in NO<sub>x</sub> reduction reactions (13)–(19), providing a pathway for NO<sub>x</sub> reduction that can improve the N<sub>2</sub> selectivity.

## 5. Conclusions

- (1) Hybrid catalysts of the type CoMn + PBA and CoMn-K + PBA exhibit better NO<sub>x</sub> storage capacity compared to PBA. This is attributed to the superior NO oxidation activity of the CoMn component relative to PBA. Additionally, XRD data suggest the Ba phase undergoes re-dispersion upon calcination of the mixtures, such that the proximity of the oxidation component (CoMn and CoMn-K) to the NO<sub>x</sub> storage sites (Ba) should facilitate NO<sub>x</sub> and O<sub>2</sub> spillover. The addition of CoMn-K also helps to mitigate the effects of sulfur poisoning.
- (2) The introduction of K<sup>+</sup> ions into the CoMn component not only increases NO oxidation activity and NO<sub>x</sub> storage efficiency due to the presence of an increased amount of surface oxygen on the catalyst, but also greatly improves the NO<sub>x</sub> reduction activity and helps to suppress N<sub>2</sub>O formation. This is explained by the fact that promotion with K<sup>+</sup> maintains the Pd in the metallic state.
- (3) By utilizing an H<sub>2</sub>-plasma in rich phase, NSR activity and N<sub>2</sub> selectivity are improved at low temperatures. This is attributed to the radical species generated by the NTP and the ability of the formed H, NH<sub>2</sub>, NH and Ar<sup>\*</sup> species to directly participate in NO<sub>x</sub> reduction reactions.

## Acknowledgements

The work was supported by the National Key R&D Program of China (No. 2017YFA0700103), and National Natural Foundation of China (Nos. 21577013 and 21707015).

## Appendix A. Supplementary data

Supplementary material related to this article can be found, in the online version, at doi:<https://doi.org/10.1016/j.apcatb.2019.01.095>.

## References

[1] Y. Ji, T. Toops, J. Pihl, M. Crocker, NO<sub>x</sub> storage and reduction in model lean NO<sub>x</sub> trap catalysts studied by *in situ* DRIFTS, *Appl. Catal. B: Environ.* 91 (2009) 329–338.

[2] C. Shi, Y. Ji, U. Graham, G. Jacobs, M. Crocker, Z. Zhang, Y. Wang, T. Toops, NO<sub>x</sub> storage and reduction properties of model ceria-based lean NO<sub>x</sub> trap catalysts, *Appl. Catal. B: Environ.* 119–120 (2012) 183–196.

[3] Z. Bai, Z. Zhang, B. Chen, Q. Zhao, M. Crocker, C. Shi, Non-thermal plasma enhanced NSR performance over Pt/M/Ba/Al<sub>2</sub>O<sub>3</sub> (M = Mn, Co, Cu) catalysts, *Chem. Eng. J.* 314 (2017) 688–699.

[4] J. Theis, An assessment of Pt and Pd model catalysts for low temperature NO<sub>x</sub> adsorption, *Catal. Today* 267 (2016) 93–109.

[5] Y. Ji, S. Bai, M. Crocker, Al<sub>2</sub>O<sub>3</sub>-based passive NO<sub>x</sub> adsorbers for low temperature applications, *Appl. Catal. B: Environ.* 170–171 (2015) 283–292.

[6] N.P. Le, X. Courtois, F. Can, S. Royer, P. Marecot, D. Duprez, NO<sub>x</sub> removal efficiency and ammonia selectivity during the NO<sub>x</sub> storage-reduction process over Pt/BaO(Fe, Mn, Ce)/Al<sub>2</sub>O<sub>3</sub> model catalysts. Part I: influence of Fe and Mn addition, *Appl. Catal. B: Environ.* 102 (2011) 353–361.

[7] J. Kim, H. Lee, M. Lee, J. Lee, J. Kim, J. Jeon, S. Jeong, S. Yoo, S. Kim, Effect of Co and Rh promoted on NO<sub>x</sub> storage and reduction over Pt/BaO/Al<sub>2</sub>O<sub>3</sub> catalyst, *J. Ind. Eng. Chem.* 14 (2008) 841–846.

[8] Z. Zhang, B. Chen, X. Wang, L. Xu, C. Au, C. Shi, M. Crocker, NO<sub>x</sub> storage and reduction properties of model manganese-based lean NO<sub>x</sub> trap catalysts, *Appl. Catal. B: Environ.* 165 (2015) 232–244.

[9] Z. Zhang, M. Crocker, L. Yu, X. Wang, Z. Bai, C. Shi, Non-thermal plasma assisted NO<sub>x</sub> storage and reduction over a cobalt-containing Pd catalyst using H<sub>2</sub> and/or CO as reductants, *Catal. Today* 258 (2015) 175–182.

[10] Z. Zhang, C. Shi, Z. Bai, M. Li, B. Chen, M. Crocker, Low-temperature H<sub>2</sub>-plasma-assisted NO<sub>x</sub> storage and reduction over a combined Pt/Ba/Al and LaMnFe catalyst, *Catal. Sci. Technol.* 7 (2017) 145–158.

[11] Z. Zhang, M. Crocker, B. Chen, Z. Bai, X. Wang, C. Shi, Pt-free, non-thermal plasma-assisted NO<sub>x</sub> storage and reduction over M/Ba/Al<sub>2</sub>O<sub>3</sub> (M = Mn, Fe, Co, Ni, Cu) catalysts, *Catal. Today* 256 (2015) 115–123.

[12] X. Wang, Y. Yu, H. He, Effect of Co addition to Pt/Ba/Al<sub>2</sub>O<sub>3</sub> system for NO<sub>x</sub> storage and reduction, *Appl. Catal. B: Environ.* 100 (2010) 19–30.

[13] Y. Huang, W. Fan, B. Long, H. Li, W. Qiu, F. Zhao, Y. Tong, H. Ji, Alkali-modified non-precious metal 3D-NiCo<sub>2</sub>O<sub>4</sub> nanosheets for efficient formaldehyde oxidation at low temperature, *J. Mater. Chem. A* 4 (2016) 3648–3654.

[14] J. Wang, J. Li, P. Zhang, G. Zhang, Understanding the “seesaw effect” of inter-layered K<sup>+</sup> with different structure in manganese oxides for the enhanced formaldehyde oxidation, *Appl. Catal. B: Environ.* 224 (2018) 863–870.

[15] Z. Hu, K. Sun, W. Li, B. Xu, NO<sub>x</sub> storage and reduction performance of Pt-CoO<sub>x</sub>–BaO/Al<sub>2</sub>O<sub>3</sub> catalysts: effects of cobalt loading and calcination temperature, *Catal. Today* 158 (2010) 432–438.

[16] Y. Wang, X. Zhu, M. Crocker, B. Chen, C. Shi, A comparative study of the catalytic oxidation of HCHO and CO over Mn<sub>0.75</sub>Co<sub>0.25</sub>O<sub>4</sub> catalyst: the effect of moisture, *Appl. Catal. B: Environ.* 160–161 (2014) 542–551.

[17] Z. Fan, Z. Zhang, W. Fang, X. Yao, G. Zou, W. Wang, Low-temperature catalytic oxidation of formaldehyde over Co<sub>3</sub>O<sub>4</sub> catalysts prepared using various precipitants, *Chin. J. Catal.* 37 (2016) 947–954.

[18] F. Xu, Z. Huang, P. Hu, Y. Chen, L. Zheng, J. Gao, X. Tang, The promotion effect of isolated potassium atoms with hybridized orbitals in catalytic oxidation, *Chem. Commun. (Camb.)* 51 (2015) 9888–9891.

[19] W. Epling, L. Campbell, A. Yezers, N. Currier, J. Parks, Overview of the fundamental reactions and degradation mechanisms of NO<sub>x</sub> storage/reduction catalysts, *Catal. Rev.* 46 (2004) 163–245.

[20] Q.H. Zhang, X.H. Liu, W.Q. Fan, Y. Wang, Manganese-promoted cobalt oxide as efficient and stable non-precious metal catalyst for preferential oxidation of CO in H<sub>2</sub> stream, *Appl. Catal. B: Environ.* 102 (2011) 207–214.

[21] F. Morales, D. Grandjean, A. Mens, F.M.F. de Groot, B.M. Weckhuysen, X-ray absorption spectroscopy of Mn/Co/TiO<sub>2</sub> Fischer–Tropsch catalysts: relationships between preparation method, molecular structure, and catalyst performance, *J. Phys. Chem. B* 110 (2006) 8626–8639.

[22] T. Zhang, R. Qu, W. Su, J. Li, A novel Ce-Ta mixed oxide catalyst for the selective catalytic reduction of NO<sub>x</sub> with NH<sub>3</sub>, *Appl. Catal. B: Environ.* 176–177 (2015) 338–346.

[23] S. Rousseau, S. Lorient, P. Delichere, A. Boreave, J. Deloume, P. Vernoux, La<sub>(1-x)</sub>Sr<sub>x</sub>Co<sub>1-x</sub>Fe<sub>y</sub>O<sub>3</sub> perovskites prepared by sol-gel method: characterization and relationships with catalytic properties for total oxidation of toluene, *Appl. Catal. B: Environ.* 88 (2009) 438–447.

[24] B. Bai, J. Li, Positive effects of K<sup>+</sup> ions on three-dimensional mesoporous Ag/Co<sub>3</sub>O<sub>4</sub> catalyst for HCHO oxidation, *ACS Catal.* 4 (2014) 2753–2762.

[25] V. O’Shea, M. Álvarez-Galván, J. Fierro, P. Arias, Influence of feed composition on the activity of Mn and PdMn/Al<sub>2</sub>O<sub>3</sub> catalysts for combustion of formaldehyde/methanol, *Appl. Catal. B: Environ.* 57 (2005) 191–199.

[26] G. Qi, R.T. Yang, Characterization and FTIR studies of MnO<sub>x</sub>–CeO<sub>2</sub> catalyst for low-temperature selective catalytic reduction of NO with NH<sub>3</sub>, *J. Phys. Chem. B* 108 (2004) 15738–15747.

[27] H. Zhao, X. Zhou, W. Huang, L. Pan, M. Wang, Q. Li, J. Shi, H. Chen, Effect of potassium nitrate modification on the performance of copper-manganese oxide catalyst for enhanced soot combustion, *ChemCatChem* 10 (2018) 1455–1463.

[28] H. Zhu, Z. Qin, W. Shan, W. Shen, J. Wang, Pd/CeO<sub>2</sub>–TiO<sub>2</sub> catalyst for CO oxidation at low temperature: a TPR study with H<sub>2</sub> and CO as reducing agents, *J. Catal.* 225 (2004) 267–277.

[29] T. Tabakova, F. Bocuzzi, M. Manzoli, D. Andreeva, FTIR study of low-temperature water-gas shift reaction on gold/ceria catalyst, *Appl. Catal. A: Gen.* 252 (2003) 385–397.

[30] S. Hilaire, X. Wang, T. Luo, R.J. Gorte, J. Wagner, A comparative study of water-gas-shift reaction over ceria supported metallic catalysts, *Appl. Catal. A: Gen.* 215 (2001) 271–278.

[31] A. Martínez-Arias, M. Fernández-García, A. Iglesias-Juez, A. Hungría, J. Anderson, J. Conesa, J. Soria, New Pd/Ce<sub>1-x</sub>Q<sub>x</sub>/Al<sub>2</sub>O<sub>3</sub> three-way catalysts prepared by microemulsion: Part 2. In situ analysis of CO oxidation and NO reduction under stoichiometric CO + NO + O<sub>2</sub>, *Appl. Catal. B: Environ.* 31 (2001) 51–60.

[32] Z. Bai, B. Chen, L. Yu, Q. Zhao, M. Crocker, C. Shi, The function of Pt in plasma-assisted NO<sub>x</sub> storage and reduction, *Catal. Commun.* 102 (2017) 81–84.

[33] Z. Zhang, M. Crocker, X. Wang, Z. Bai, C. Shi, Non-thermal plasma-assisted NO<sub>x</sub> storage and reduction over cobalt-containing LNT catalysts, *Catal. Today* 258 (2015) 386–395.

[34] H. Abdulhamid, E. Fridell, J. Dawody, M. Skoglundh, In situ FTIR study of SO<sub>2</sub> interaction with Pt/BaCo<sub>3</sub>/Al<sub>2</sub>O<sub>3</sub> NO<sub>x</sub> storage catalysts under lean and rich conditions, *J. Catal.* 241 (2006) 200–210.

[35] L. Kylhammar, P. Carlsson, H. Ingelsten, H. Gronbeck, M. Skoglundh, Regenerable ceria-based SO<sub>x</sub> traps for sulfur removal in lean exhausts, *Appl. Catal. B: Environ.* 84 (2008) 268–276.

[36] Y. Zhang, Y. Yu, H. He, Oxygen vacancies on nanosized ceria govern the NO<sub>x</sub> storage capacity of NSR catalysts, *Catal. Sci. Technol.* 6 (2016) 3950–3962.

[37] T. Toops, D. Smith, W. Partridge, Quantification of the in situ DRIFT spectra of Pt/K/γ-Al<sub>2</sub>O<sub>3</sub> NO<sub>x</sub> adsorber catalysts, *Appl. Catal. B: Environ.* 58 (2005) 245–254.

[38] T. Dang, D. Yoon, C. Kim, Synthesis of AlN whiskers using cobalt oxide catalyst and their alignments for the improvement of thermal conductivity, *Mater. Chem. Phys.* 179 (2016) 204–213.

[39] F. Kabbany, G. Said, Y. Badr, S. Taha, Infrared investigation of the phase transition in K<sub>2</sub>SO<sub>4</sub>, *Phys. Status Solidi A* 67 (1981) 339–345.

[40] R. Matarrese, L. Castoldi, N. Artioli, E. Finocchio, G. Busca, L. Lietti, On the activity and stability of Pt-K/Al<sub>2</sub>O<sub>3</sub> LNT catalysts for diesel soot and NO<sub>x</sub> abatement, *Appl. Catal. B: Environ.* 144 (2014) 783–791.

[41] L. Righini, F. Gao, L. Lietti, J. Szanyi, C.H.F. Peden, Performance and properties of K and TiO<sub>2</sub> based LNT catalysts, *Appl. Catal. B: Environ.* 181 (2016) 862–873.

[42] R. Vijay, R. Hendershot, S. Rivera-Jiménez, W. Rogers, B. Feist, C. Snively, J. Lauterbach, Noble metal free NO<sub>x</sub> storage catalysts using cobalt discovered via high-throughput experimentation, *Catal. Commun.* 6 (2005) 167–171.

[43] R. Clayton, M. Harold, V. Balakotaiah, C. Wan, Pt dispersion effects during NO<sub>x</sub> storage and reduction on Pt/BaO/Al<sub>2</sub>O<sub>3</sub> catalysts, *Appl. Catal. B: Environ.* 90 (2009) 662–676.

[44] D. Kim, A. Yezers, J. Li, N. Currier, H. Chen, H. Hess, M. Engelhard, G. Muntean, C. Peden, Effect of sulfur loading on the desulfation chemistry of a commercial lean NO<sub>x</sub> trap catalyst, *Catal. Today* 197 (2012) 3–8.

[45] L. Castoldi, I. Nova, L. Lietti, P. Forzatti, Study of the effect of Ba loading for catalytic activity of Pt-Ba/Al<sub>2</sub>O<sub>3</sub> model catalysts, *Catal. Today* 96 (2004) 43–52.

[46] L. Cumaranatunge, S. Mulla, A. Yezers, N. Currier, W. Delgass, F. Ribeiro, Ammonia is a hydrogen carrier in the regeneration of Pt/BaO/Al<sub>2</sub>O<sub>3</sub> NO<sub>x</sub> traps with H<sub>2</sub>, *J. Catal.* 246 (2007) 29–34.

[47] J. Pihl, P. Parks, C. Daw, T. Root, Product Selectivity During Regeneration of Lean NO<sub>x</sub> Trap Catalysts, SAE International, 2006.

[48] Q. Yu, H. Wang, T. Liu, L. Xiao, X. Jiang, X. Zheng, High-efficiency removal of NO<sub>x</sub> using a combined adsorption-discharge plasma catalytic process, *Environ. Sci. Technol.* 46 (2012) 2337–2344.

[49] H. Wang, X. Li, P. Chen, M. Chen, X. Zheng, An enhanced plasma-catalytic method for DeNO<sub>x</sub> in simulated flue gas at room temperature, *Chem. Commun.* 49 (2013) 9353–9355.

[50] J. Park, I. Tomicic, G. Round, J. Chang, Simultaneous removal of NO<sub>x</sub> and SO<sub>2</sub> from NO–SO<sub>2</sub>–CO<sub>2</sub>–N<sub>2</sub>–O<sub>2</sub> gas mixtures by corona radical shower systems, *J. Phys. D: Appl. Phys.* 32 (1999) 1006.

[51] K. Yan, S. Kanazawa, T. Ohkubo, Y. Nomoto, Oxidation and reduction processes during NO<sub>x</sub> removal with corona-induced nonthermal plasma, *Plasma Chem. Plasma Process.* 19 (1999) 421–443.